

# Performance Analysis of Real-Time Detection in Fusion-based Sensor Networks

Rui Tan, *Student Member, IEEE*, Guoliang Xing, *Member, IEEE*,  
Jianping Wang, *Member, IEEE*, Benyuan Liu, *Member, IEEE*

**Abstract**—Real-time detection is an important requirement of many mission-critical wireless sensor network applications such as battlefield monitoring and security surveillance. Due to the high network deployment cost, it is crucial to understand and predict the real-time detection capability of a sensor network. However, most existing real-time analyses are based on overly simplistic sensing models (e.g., the disc model) that do not capture the stochastic nature of detection. In practice, data fusion has been adopted in a number of sensor systems to deal with sensing uncertainty and enable efficient collaboration among resource-limited sensors. However, real-time performance analysis of sensor networks designed based on data fusion has received little attention. In this paper, we bridge this gap by investigating the fundamental real-time detection performance of large-scale sensor networks under stochastic sensing models. In particular, we consider two basic data fusion schemes, i.e., value fusion and decision fusion. Our results show that data fusion is effective in achieving stringent performance requirements such as short detection delay and low false alarm rates. Moreover, value fusion and decision fusion are suitable for low and high signal-to-noise ratio scenarios, respectively. Our results help understand the impact of data fusion and provide important guidelines for the design of real-time wireless sensor networks for intrusion detection. Our analyses are verified through extensive simulations based on both synthetic data sets and data traces collected in a real deployment for vehicle detection. The results show that data fusion can reduce the network density by about 60% compared with the disc model while detecting any intruder within one detection period at a false alarm rate lower than 5%.

**Index Terms**—Data fusion, real-time intrusion detection, performance limits, wireless sensor networks.

## 1 INTRODUCTION

WIRELESS sensor networks are increasingly available for mission-critical applications such as battlefield monitoring and security surveillance. A fundamental objective of these applications is *real-time intrusion detection* that requires any unknown intruders to be detected by the network within tight deadlines. Many intrusion detection scenarios involve a large number of sensors distributed in a vast geographical area. Moreover, sensor nodes are often not accessible after deployment due to the constraints of physical environments (e.g., battlefields). Therefore, it is crucial to analyze and understand the expected real-time performance of WSNs before the actual deployment.

However, we face several key challenges in analyzing the real-time performance of sensor networks for intrusion detection. First, the real-time detection performance of a sensor network is inherently affected by the uncertainties in network deployment and sensor measurement. For instance, unpredictable environmental noises can easily trigger false alarms of low-cost sensors, resulting probabilistic detection performance. Although false alarms can be suppressed by making sensors more conservative, it inevitably jeopardizes the timeliness of

detection. Therefore, there exist fundamental trade-offs between real-time and other detection performance metrics of a sensor network. Second, the adoption of advanced signal processing algorithms often significantly complicates the modeling and analysis of system real-time performance. Collaborative signal processing techniques such as data fusion [1] are widely employed by current sensor systems to enable the cooperation among multiple sensors with limited sensing capability. For instance, reliable intrusion detection in noisy environments requires the aggregation of readings from multiple sensors [2]. However, such requirements often have complex impacts on the system real-time performance.

Recently, several sensor networks have been developed for real-time detection [3], [4]. However, the real-time performance of such systems are often analyzed based on *overly simplistic* sensing models [3]–[10]. In particular, the sensing region of a sensor is modeled as a disc with radius  $r$  centered at the position of the sensor, where  $r$  is referred to as the *sensing range*. A sensor *deterministically* detects the targets within its sensing range. As this simplistic disc model allows a geometric treatment to the detection problem, it has been widely adopted in the design and analysis of surveillance sensor networks. However, a key shortcoming of the disc model is that it fails to capture the stochastic nature of sensing, such as probabilistic delay and detectability caused by noise. Moreover, most studies based on the disc model do not exploit the collaboration among sensors.

To illustrate the inaccuracy of the disc model, we plot the sensing performance of an acoustic sensor in

- R. Tan and G. Xing are with Department of Computer Science and Engineering, Michigan State University, East Lansing, MI 48824, USA. E-mail: tanrui@ieee.org, glxing@msu.edu
- J. Wang is with Department of Computer Science, City University of Hong Kong, Kowloon, Hong Kong. E-mail: jianwang@cityu.edu.hk
- B. Liu is with Department of Computer Science, University of Massachusetts Lowell, Lowell, MA 01854, USA. E-mail: bliu@cs.uml.edu

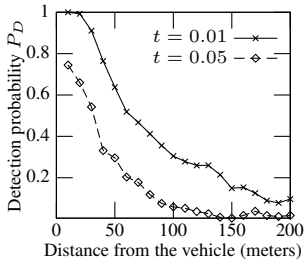


Fig. 1. Detection probability versus the distance from the vehicle.

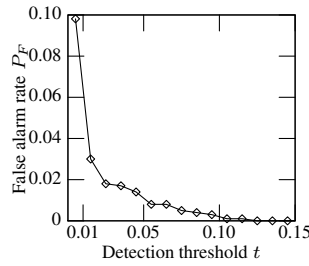


Fig. 2. False alarm rate versus detection threshold.

Fig. 1 and 2 using the data traces collected in a vehicle detection experiment [11]. In the experiment, the sensor detects moving vehicles by comparing its signal energy measurement against a threshold (denoted by  $t$ ). Fig. 1 plots the probability that the sensor detects a vehicle (denoted by  $P_D$ ) versus the distance from the vehicle. No clear cut-off boundary between successful and unsuccessful sensing of the target can be seen in Fig. 1. Similar result is observed for the sensor's false alarm rate (denoted by  $P_F$ ) and the detection threshold shown in Fig. 2. Note that  $P_F$  is the probability of making a positive decision when *no* vehicle is present.

In this work, we develop an analytical framework to study the real-time surveillance performance of large-scale WSNs that are designed based on collaborative data fusion algorithms. To quantify the fundamental trade-off between detection delay and false alarm rate, we propose a new real-time metric called  $\alpha$ -delay that is defined as the delay of detecting an intruder subject to the false alarm rate bound  $\alpha$ . Compared with the classical definition of detection delay,  $\alpha$ -delay explicitly captures the probabilistic detection performance caused by stochastic sensing. In particular, as many mission-critical real-time applications require detection delay to be as small as possible, we are interested in the asymptotic case where  $\alpha$ -delay is minimized, i.e., any intruder can be detected almost surely once after its appearance, while the false alarm rate is no greater than  $\alpha$ .

The main focus of this paper is to establish the correlation between network density and  $\alpha$ -delay in real-time intrusion detection. To our best knowledge, this work is the first to study the real-time performance of large-scale WSNs based on collaborative sensing models. Our results help understand the limitations of the existing real-time analyses based on simplistic sensing models, and provide key insights into designing and analyzing the large-scale WSNs that adopt data fusion algorithms. The main contributions of this paper are as follows.

- We derive the  $\alpha$ -delay of random networks under both data fusion and probabilistic disc models. These results can be used to achieve desirable trade-offs between false alarm rate, detection delay and network density. In particular, we consider two basic data fusion schemes, i.e., value fusion and deci-

sion fusion. Moreover, the existing analytical results based on the disc model can be naturally extended to the context of stochastic event detection.

- To understand the limitation of the disc model and the impacts of data fusion on real-time detection, we conduct comparative analysis between the disc and fusion-based sensing models. We show that the ratio of network densities to achieve the minimum  $\alpha$ -delay under the two models has an asymptotic upper bound of  $\mathcal{O}\left(e^{-\psi \cdot \text{SNR}} \cdot \left(\frac{\text{SNR}}{Q^{-1}(\alpha)}\right)^{2/k}\right)$ , where  $k$  is the signal path loss exponent,  $Q^{-1}(\cdot)$  is the inverse  $Q$ -function of the standard normal distribution,  $\psi = 0$  and  $\psi = 1$  for value and decision fusion models, respectively. The result implies that data fusion is effective in achieving stringent performance requirements such as short detection delay and low false alarm rate. Moreover, value and decision fusion models are suitable for low and high signal-to-noise ratio (SNR) scenarios, respectively.
- We conduct extensive simulations based on both synthetic data sets and data traces collected in a real deployment for vehicle detection. The results show that data fusion can reduce the network density by about 60% compared with the disc model while detecting any intruder within one detection period at a false alarm rate lower than 5%. Moreover, the data fusion models are more robust than the disc model in detecting slowly moving targets.

The rest of this paper is organized as follows. Section 2 reviews related work. Section 3 introduces the preliminaries and problem definition. In Section 4 and 5, we derive the  $\alpha$ -delay under the disc and fusion models, respectively. In Section 6, we study the impact of data fusion on real-time detection through performance comparison between the two models. In Section 7, we extend the analyses to address arbitrary target speed and decision fusion. Section 8 presents simulation results and Section 9 concludes this paper.

## 2 RELATED WORK

Most existing real-time analyses of target detection [5]–[7] and sensing coverage [8]–[10] in WSNs are based on the simplistic disc model. The delay of detecting a moving target with randomly deployed sensors has been analyzed in [5], [6]. The length of free path that a target travels undetected is derived in [7]. However, the disc model adopted by these works fails to capture the stochastic characteristics of real-world intrusion detection, such as probabilistic detectability and false alarms. In this paper, we study the relationship between the performance of real-time stochastic detection and network density. We propose a probabilistic disc model that naturally extends the existing analytical results [9] based on the classical disc model to the context of stochastic detection. In [12], we developed data fusion algorithms for volcanic earthquake detection using wireless sensor systems. Moreover, we study the impact of data fusion

on network density and compare with the results under the probabilistic disc model.

Many sensor network systems have incorporated various data fusion schemes to improve the system performance [2], [11], [13]–[18]. In the surveillance system based on MICA2 motes developed in [2], the system false alarm rate is reduced by fusing the detection decisions made by multiple neighboring sensors. In the DARPA/IXOs SensIT project, advanced data fusion techniques have been employed in a number of algorithms and protocols designed for target detection [13]–[15], localization [16], [17], and classification [11], [18]. In our recent work, we have developed static sensor deployment algorithms [19] and mobile sensor scheduling algorithms [20], [21] for fusion-based target detection in WSNs. However, the performance analysis of large-scale fusion-based WSNs has received little attention.

There is vast literature on stochastic signal detection based on multi-sensor data fusion. Early work [1] focuses on small-scale powerful sensor networks (e.g., several radars). Recent studies on data fusion [14], [15], [22] have considered the specific properties of WSNs such as sensors' spatial distribution and limited sensing capability. However, these works focus on analyzing the optimal fusion strategies that maximize the system detection performance of a given network. Our recent work [23] investigates the fundamental impacts of data fusion on the coverage of static targets in WSNs. In contrast, this paper studies the impact of data fusion on the delay of detecting mobile targets.

### 3 PRELIMINARIES AND PROBLEM DEFINITION

In this section, we first describe the preliminaries of our work, which include sensor measurement, network, and data fusion models. We then introduce the problem definition.

#### 3.1 Sensor Measurement and Network Models

Sensors perform detection by measuring the energy of signals emitted by the target.<sup>1</sup> The energy of most physical signals (e.g., acoustic and electromagnetic signals) attenuates with the distance from the signal source. Suppose sensor  $i$  is  $d_i$  meters away from the target that emits a signal of energy  $S$ . The attenuated signal energy  $s_i$  at the position of sensor  $i$  is given by  $s_i = S \cdot w(d_i)$ , where  $w(\cdot)$  is a decreasing function satisfying  $w(0) = 1$ ,  $w(\infty) = 0$  and  $w(x) = \Theta(x^{-k})$ .<sup>2</sup> Depending on the environment, e.g., atmosphere conditions, the signal's path loss exponent  $k$  typically ranges from 2.0 to 5.0 [17], [24]. The  $w(\cdot)$  is referred to as the *signal decay function*. We

1. Several types of sensors (e.g., acoustic sensor) only sample signal intensity at a given sampling rate. The *signal energy* can be obtained by preprocessing the time series during a period, which has been commonly adopted to avoid the transmission of raw data [11], [14]–[17].

2. We adopt the following asymptotic notation: 1)  $f(x) = \Theta(g(x))$  means that  $g(x)$  is the asymptotic tight bound of  $f(x)$ ; 2)  $f(x) = \mathcal{O}(g(x))$  means that  $g(x)$  is the asymptotic upper bound of  $f(x)$ .

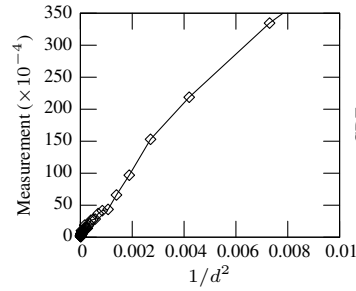


Fig. 3. Energy measurement versus  $1/d^2$  ( $d$  is the distance from the target, in unit of meters).

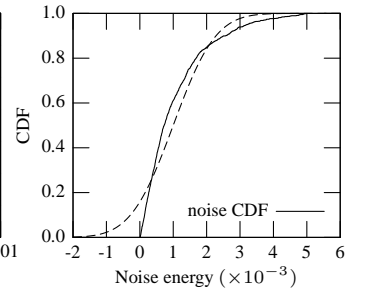


Fig. 4. The CDF of noise energy. The dashed line is the CDF of the unit of meters.  $\mathcal{N}(0.001, 0.001^2)$ .

note that the theoretical results derived in this paper do not depend on the closed-form formula of the  $w(\cdot)$ . We adopt  $w(x) = \frac{1}{1+x^k}$  in the simulations conducted in this paper, and we set  $k = 2$  except those explicitly specified.

The measurements of sensors are contaminated by additive random noises from sensor hardware or environment. Depending on the hypothesis that the target is absent ( $H_0$ ) or present ( $H_1$ ), the measurement of sensor  $i$ , denoted by  $y_i$ , is given by

$$H_0 : y_i = n_i, \quad H_1 : y_i = s_i + n_i,$$

where  $n_i$  is the energy of noise experienced by sensor  $i$ . We assume that the noise  $n_i$  at each sensor  $i$  follows the normal distribution, i.e.,  $n_i \sim \mathcal{N}(\mu, \sigma^2)$ , where  $\mu$  and  $\sigma^2$  are the mean and variance of  $n_i$ , respectively. We assume that the noises,  $\{n_i | \forall i\}$ , are spatially independent across sensors. Therefore, the noises at sensors are independent and identically distributed (*i.i.d.*) Gaussian noises. In the presence of target, the measurement of sensor  $i$  follows the normal distribution, i.e.,  $y_i | H_1 \sim \mathcal{N}(s_i + \mu, \sigma^2)$ . Due to the independence of noises, the sensors' measurements,  $\{y_i | \forall i, H_1\}$ , are spatially independent but *not* identically distributed as sensors receive different signal energies from the target. In this paper, we define the SNR as  $\delta = S/\sigma$  which quantifies the noise level.

The above signal decay and sensor measurement models have been widely assumed in the literature of signal detection [1], [9], [13], [15], [16], [22], [23] and also have been empirically verified [17], [24]. Fig. 3 and Fig. 4 plot the energy of signal from driving vehicles and noise measured by an acoustic sensor in the SensIT experiments [11]. From Fig. 3, we can see that the signal energy increases linearly with  $1/d^2$ , which indicates that  $w(x)$  has an order of  $x^{-2}$ . This is consistent with the signal decay model adopted in this paper with  $k = 2$ . Fig. 4 plots the cumulative distribution function (CDF) of noise energy, which matches the CDF of the normal distribution.

We assume that a sensor executes detection task every  $T$  seconds.  $T$  is referred to as the *detection period*. In each detection period, a sensor gathers the signal energy during the *sampling interval* for the detection made in the

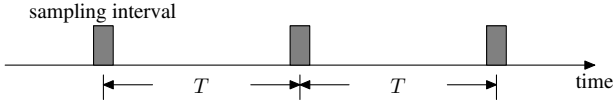


Fig. 5. Temporal view of a single sensor's operation. The sensor outputs an energy measurement after each sampling interval.

current period. The temporal view of a single sensor's operation is illustrated in Fig. 5. We note that such an intermittent measurement scheme is consistent with several wireless sensor systems for target detection and tracking [2], [11], [14]. For instance, a sensor may wake up every 5 seconds and sample acoustic energy for 0.05 seconds, where  $T$  is 5s and the sampling interval is 0.05 s [11]. We assume that the sampling interval is much shorter than the detection period.

We consider a network deployed in a vast two-dimensional geographical region. Several recent projects have demonstrated the deployment of large-scale sensor networks. In the ExScal project [4], [25], about 1200 nodes are distributed in an area of 1.3 km by 300 m. We assume that the positions of sensors are uniformly and independently distributed in the deployment region. Such a deployment scenario can be modeled as a stationary two-dimensional Poisson point process. Let  $\rho$  denote the density of the underlying Poisson point process. We note that such a deployment model has been widely assumed to analyze the performance of large-scale sensor networks [5]–[9]. Adopting this model thus allows us to directly compare our results with the existing results.

We assume that the target may appear at any location in the deployment region and move freely. Moreover, the target is blind to the network, i.e., the target does not know the sensors' positions, and hence it cannot choose a moving scheme to reduce the probability of being detected. The sensors synchronously detect the target, and we refer to the target detection in one detection period as the *unit detection*. The process of detecting a target consists of a series of unit detections. As the sampling interval is much shorter than the detection period, we ignore the target's movement during the sampling interval.

Table 1 summarizes the notation used in this paper.

### 3.2 Data Fusion Model

Data fusion [1] can improve the performance of detection systems by jointly considering the noisy measurements of multiple sensors. There exist two basic data fusion schemes, namely, *decision fusion* and *value fusion*. In value fusion [15], each sensor sends its energy measurements to the cluster head, which makes a decision based on the measurements. In decision fusion [22], each sensor makes a local decision based on its measurement and sends its decision to the cluster head, which makes a system decision according to the local decisions. In this

TABLE 1  
Summary of Notation

| Symbol          | Definition   |
|-----------------|--|
| $S$             | original energy emitted by the target                    |
| $\mu, \sigma^2$ | mean and variance of noise energy                        |
| $\delta$        | signal-to-noise ratio (SNR), $\delta = S/\sigma$         |
| $d_i$           | distance from the target                                 |
| $w(\cdot)$      | signal decay function, $w(x) = \Theta(x^{-k})$           |
| $s_i$           | attenuated signal energy, $s_i = S \cdot w(d_i)$         |
| $n_i$           | noise energy, $n_i \sim \mathcal{N}(\mu, \sigma^2)$      |
| $H_0 / H_1$     | hypothesis that the target is absent / present           |
| $y_i$           | energy measurement, $y_i H_0 = n_i, y_i H_1 = s_i + n_i$ |
| $\alpha$        | upper bound of false alarm rate                          |
| $\rho$          | network density  |
| $\mathbf{F}(P)$ | the set of sensors within fusion range of point $P$      |
| $N(P)$          | the number of sensors in $\mathbf{F}(P)$                 |

\* The symbols with subscript  $i$  refer to the notation of sensor  $i$ .

paper, we first focus on value fusion and then extend the results to decision fusion in Section 7. As proved in [23], the optimal value fusion rule is to compare the weighted sum of measurements,  $\sum_i \frac{s_i}{\sigma} \cdot y_i$ , against a threshold. However, as the measurements contain both noise and signal energy, the weight  $\frac{s_i}{\sigma}$ , i.e., the received SNR of sensor  $i$ , is often unknown in practice. A practical solution is to adopt equal constant weights for all sensors' measurements [15], [22], [23]. Since the measurements from different sensors are treated equally, the sensors far away from the target should be excluded from data fusion as their measurements suffer low received SNRs. Hence, we adopt a value fusion model as follows.

For any physical point  $P$ , the sensors within a distance of  $R$  meters from  $P$  participate in the data fusion to detect whether a target is present at  $P$ .  $R$  is referred to as the *fusion range* and  $\mathbf{F}(P)$  denotes the set of sensors within the fusion range of  $P$ . The number of sensors in  $\mathbf{F}(P)$  is represented by  $N(P)$ . For conciseness, we use  $\mathbf{F}$  for  $\mathbf{F}(P)$  and  $N$  for  $N(P)$  when the point of interest is clear. Due to the Poisson process deployment, for a random point  $P$ ,  $N$  follows the Poisson distribution with mean of  $\rho\pi R^2$ , i.e.,  $N \sim \text{Poi}(\rho\pi R^2)$ . In each detection period, a cluster head is elected to make the detection decision by comparing the sum of measurements reported by member sensors within the fusion range against a detection threshold  $\eta$ . Let  $Y$  denote the sum of measurements, i.e.,  $Y = \sum_{i \in \mathbf{F}} y_i$ . If  $Y \geq \eta$ , the cluster head decides  $H_1$ ; otherwise, it decides  $H_0$ . Fig. 6 illustrates the intrusion detection under the data fusion model.

We assume that the system can obtain the position of a possible target through a localization service in the network [16], [17]. An analysis based on a simple localization algorithm shows that the localization error decreases with network density and becomes insignificant when the network density is high enough. The details of the analysis are in Appendix A, which can be found in the supplemental materials of this paper.

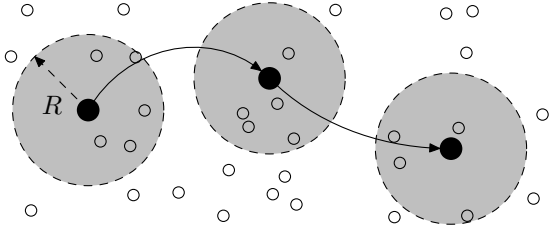


Fig. 6. Intrusion detection under data fusion model. The void circles represent randomly deployed sensors; the solid circles represent the target in different sampling intervals; the dashed discs represent the fusion ranges.

Under such an assumption, the localization error can be safely ignored in our analysis that is focused on the detection delay when the network density is high. We also evaluate the impact of localization error through simulations in Section 8.

In each detection period, a cluster is formed by the sensors within the fusion range centered at the possible target to make a detection decision. The cluster formation may be initiated by the sensor that has the maximum measurement. Such a scheme can be implemented by several dynamic clustering algorithms [26]. The fusion range  $R$  can be used as an input parameter of the clustering algorithm.

### 3.3 Problem Definition

In this paper, we study the delay of stochastic intrusion detection in large-scale sensor networks. As the process of detecting a target is inherently stochastic, the detection delay is closely related to two system performance metrics, namely, the false alarm rate (denoted by  $P_F$ ) and detection probability (denoted by  $P_D$ ).  $P_F$  is the probability of making a positive decision when no target is present, and  $P_D$  is the probability that a present target is correctly detected. In stochastic detection, positive detection decisions may be false alarms caused by the noise in sensor measurements. Note that the false alarm rate does not depend on the property of target as it is the probability of making positive decision when *no* target is present. Although detection delay can be reduced by making sensors more sensitive (e.g., setting lower detection threshold), the fidelity of detection results may be unacceptable because of high false alarm rates caused by noises. Therefore, studying detection delay alone without the consideration of false alarm is meaningless. We now introduce a concept called  $\alpha$ -delay that quantifies the delay of detection under bounded false alarm rate.

**Definition 1.**  $\alpha$ -delay is the average number of detection periods before a target is first detected subject to that the false alarm rate of the network is no greater than  $\alpha$ , i.e.,  $P_F \leq \alpha$ , where  $\alpha \in (0, 1)$ .

In practice, mission-critical surveillance applications require a low false alarm rate ( $\alpha < 5\%$ ) [2], [27], as false alarms not only reduce the fidelity of detection results

but also waste energy in responsive operations such as waking up asleep sensors. The focus of this paper is to study the relationship between the  $\alpha$ -delay and network density. Network density directly determines the cost of constructing and deploying a network. Thus, our results will allow the network designer to achieve desirable trade-offs between cost, false alarm rate, and detection delay. Moreover, many sensor networks reduce energy consumption by only activating a subset of nodes while scheduling others to sleep [2]. Our results can be applied to reduce the density of active nodes while achieving the required detection delay. As the detection delay often dominates the communication delay in stochastic intrusion detection, we ignore the communication delay in this paper. For instance, the delay of aggregating the readings of a group of nodes is within 5 milliseconds [3] while the detection period can be several seconds.

We address the following problems in this paper:

- 1) Are the analytical results on detection delay [5]–[10] derived under the classical disc model still applicable under the definition of  $\alpha$ -delay? We propose a probabilistic disc model such that the existing results can be naturally extended to the context of stochastic detection (Section 4).
- 2) How to quantify the  $\alpha$ -delay when sensors can collaborate through data fusion? Answering this question enables us to evaluate the timeliness of a fusion-based network and to deploy the fewest sensors for achieving a given  $\alpha$ -delay (Section 5).
- 3) What is the impact of data fusion on network density when the  $\alpha$ -delay is minimized? Many mission-critical real-time applications require detection delay to be as short as possible [2], [27]. We analytically compare the network densities under the disc and fusion models when the  $\alpha$ -delay is minimized. The result provides important insights into understanding the limitation of the disc model and the impact of data fusion on the design of real-time WSNs (Section 6).

## 4 $\alpha$ -DELAY UNDER PROBABILISTIC DISC MODEL

In the classical disc model, each sensor has deterministic sensing capability within its sensing range. If the target is within at least one sensor's sensing range, the target is regarded to be detected by the network. Such a model is not consistent with the stochastic nature of signal detection. As a result, although a number of studies [5]–[10] have been conducted on intrusion detection based on the disc model, they cannot be readily used to analyze the performance or guide the design of real-world intrusion detection systems. In this section, we extend the classical disc model based on the stochastic detection theory [1] to capture several realistic sensing characteristics and study the  $\alpha$ -delay under the extended model. The result lays a foundation for understanding the limitation of disc model on quantifying the delay of intrusion detection.

#### 4.1 Probabilistic Disc Model

In the *probabilistic disc model*, we choose sensing range  $r$  such that 1) the probability of detecting any target within  $r$  meters from it is no lower than  $\beta$ , and 2) the false alarm rate is no greater than  $\alpha$ , where  $\alpha$  and  $\beta$  are parameters specified by user. Note that  $\alpha$  and  $\beta$  are both within  $(0, 1)$ . As we ignore the detection probability outside the sensing range of a sensor, the detection capability of sensor under this model is lower than in reality. However, this model preserves the *boundary* of sensing region defined in the classical disc model. Accordingly, the existing analytical results based on the classical model [5]–[10] can be naturally extended to the context of stochastic detection. In Section 4.2, we will discuss how to extend the coverage probability derived under the classical model [9] to study the  $\alpha$ -delay of stochastic intrusion detection.

We now discuss how to choose the sensing range  $r$  under the probabilistic disc model. The optimal Bayesian detection rule for a single sensor  $i$  is to compare its measurement  $y_i$  against a detection threshold  $t$  [1]. If  $y_i$  exceeds  $t$ , sensor  $i$  decides  $H_1$ ; otherwise, it decides  $H_0$ . As both  $y_i|H_0$  and  $y_i|H_1$  follow the normal distributions, i.e.,  $y_i|H_0 = n_i \sim \mathcal{N}(\mu, \sigma^2)$  and  $y_i|H_1 = s_i + n_i \sim \mathcal{N}(\mu + s_i, \sigma^2)$ , the false alarm rate and detection probability of sensor  $i$  are given by

$$P_F = \mathbb{P}(y_i \geq t|H_0) = Q\left(\frac{t - \mu}{\sigma}\right), \quad (1)$$

$$P_D = \mathbb{P}(y_i \geq t|H_1) = Q\left(\frac{t - \mu - s_i}{\sigma}\right), \quad (2)$$

where  $Q(\cdot)$  is the complementary CDF of the standard normal distribution, formally,  $Q(x) = \frac{1}{\sqrt{2\pi}} \int_x^\infty e^{-t^2/2} dt$ . To derive the sensing range, we let  $P_F = \alpha$  and  $P_D = \beta$ . The detection threshold  $t$  can then be solved from (1) as  $t = \mu + \sigma Q^{-1}(\alpha)$ , where  $Q^{-1}(\cdot)$  is the inverse function of  $Q(\cdot)$ . Moreover, by replacing  $s_i = S \cdot w(r)$  in (2), we have

$$r = w^{-1}\left(\frac{Q^{-1}(\alpha) - Q^{-1}(\beta)}{\delta}\right) \quad (3)$$

For instance, the sensing range  $r$  is 3.8 m if  $\alpha = 0.05$ ,  $\beta = 0.95$ ,  $\delta = 50$  (i.e., 17 dB) and  $w(x) = \frac{1}{1+x^2}$ .<sup>3</sup> Moreover, we can see from (3) that  $r$  increases with the SNR  $\delta$ . This conforms to the intuition that a sensor can detect a farther target if the noise level is lower (i.e., a greater  $\delta$ ). As  $Q^{-1}(\cdot)$  is a decreasing function,  $r$  will decrease if a lower false alarm rate is required (i.e., a smaller  $\alpha$ ).

#### 4.2 $\alpha$ -Delay under Probabilistic Disc Model

The intrusion detection under the probabilistic disc model works as follows. The network periodically detects the target as described in Section 3.3. In each unit detection, if the target is within at least one sensor's

sensing range, the target is detected with a probability no lower than  $\beta$ . We let  $\beta$  be sufficiently close to 1 (e.g.,  $\beta = 0.99$ ) such that the target is detected almost surely if it is within any sensor's sensing range. Such a setting enables the sensors to exhibit similar deterministic property as under the classical disc model. We refer to the circular region with radius of  $r$  centered at the target as the *target disc*. Hence, the target is detected if there is at least one sensor within the target disc. In this section, we assume that there is no overlap between any two target discs such that the unit detections are independent from each other. Such independence among unit detections can significantly simplify the analysis. We now discuss the condition for no overlap between any two target discs. Suppose the target moves at a constant speed of  $v$ , the no-overlap condition can be satisfied if  $vT > 2r$ . For instance, if the sensing range  $r$  is 3.8 m as mentioned in Section 4.1 and the target speed  $v$  is 5 m/s (i.e., 18 km/h) [11], the target discs will not overlap as long as the detection period  $T$  is greater than 2 s. In Section 7.1, we extend the analysis to the case where target discs may overlap. We have the following lemma.

**Lemma 1.** *Let  $\tau$  denote the  $\alpha$ -delay under the probabilistic disc model. If there is no overlap between any two target discs,  $\tau = \frac{1}{1 - e^{-\rho\pi r^2}}$ .*

*Proof:* As shown in [9], when the sensors are deployed according to the Poisson process, the probability that there is at least one sensor in a target disc is  $p = 1 - e^{-\rho\pi r^2}$ . Suppose the target is detected in the  $J^{\text{th}}$  ( $J \geq 1$ ) detection period. As there is no overlap between any two target discs, the unit detections are independent from each other. Therefore,  $J$  follows the geometric distribution with a success probability of  $p$  in each Bernoulli trial (i.e., each unit detection). Moreover, according to the definition of  $r$  in (3), the false alarm rate in each unit detection is no greater than  $\alpha$ . According to Definition 1, the  $\alpha$ -delay is given by  $\tau = \mathbb{E}[J] = \frac{1}{p} = \frac{1}{1 - e^{-\rho\pi r^2}}$ .  $\square$

We can see from Lemma 1 that the  $\alpha$ -delay decreases with network density  $\rho$  and sensing range  $r$ . Note that  $r$  is given by (3) under the probabilistic disc model.

### 5 $\alpha$ -DELAY UNDER DATA FUSION MODEL

Although the probabilistic disc model discussed in Section 4 captures the stochastic nature of sensing, it does not exploit the possible collaboration among sensors. In this section, we derive the detection performance and  $\alpha$ -delay under the data fusion model presented in Section 3.2.

#### 5.1 Performance Modeling of Fusion-based Detection

In this section, we derive the false alarm rate and detection probability in a unit detection. The results will be used in Section 5.2 to analyze the  $\alpha$ -delay under the fusion model.

3. The SNR is set to be 17 dB according to the measurements in the vehicle detection experiments based on MICA2 [28] and ExScal [25] notes.

When no target is present, each sensor measures *i.i.d.* noise as discussed in Section 3.1. Denote  $\mathbf{F}_j$  as the set of sensors within the fusion range in the  $j^{\text{th}}$  unit detection. Suppose there are  $N_j$  sensors in  $\mathbf{F}_j$ . The sum of energy measurements follows the normal distribution, i.e.,  $Y|H_0 = \sum_{i \in \mathbf{F}_j} n_i \sim \mathcal{N}(N_j\mu, N_j\sigma^2)$ . Therefore, the false alarm rate of the  $j^{\text{th}}$  unit detection is given by  $P_{Fj} = \mathbb{P}(Y \geq \eta|H_0) = Q\left(\frac{\eta - N_j\mu}{\sqrt{N_j}\sigma}\right)$ , where  $\eta$  is the detection threshold. As  $P_D$  is a non-decreasing function of  $P_F$  [1], it is maximized when  $P_F$  is set to be the upper bound  $\alpha$ . Such a scheme is referred to as the constant false alarm rate detector [1]. Let  $P_{Fj} = \alpha$ , the optimal detection threshold can be derived as  $\eta^* = N_j\mu + \sqrt{N_j}\sigma Q^{-1}(\alpha)$ .

When the target is present, the sum of energy measurements in the  $j^{\text{th}}$  unit detection is  $Y|H_1 = \sum_{i \in \mathbf{F}_j} s_i + \sum_{i \in \mathbf{F}_j} n_i$ . The attenuated signal energies  $\{s_i|i \in \mathbf{F}_j\}$  are *i.i.d.* and we denote  $\mu_s$  and  $\sigma_s^2$  as the mean and variance of  $s_i$ , respectively. The proof for the independence of  $\{s_i|i \in \mathbf{F}_j\}$  and the derivation of  $\mu_s$  and  $\sigma_s^2$  are in Appendix B, which can be found in the supplemental materials of this paper. The  $\mu_s$  and  $\sigma_s^2$  are given by  $\mu_s = S \cdot \mu_0$  and  $\sigma_s^2 = S^2 \cdot \sigma_0^2$ , where  $\mu_0 = \frac{2}{R^2} \int_0^R w(d_i)d_i dd_i$  and  $\sigma_0^2 = \frac{2}{R^2} \int_0^R w^2(d_i)d_i dd_i - \mu_0^2$ . If  $N_j$  is large enough,  $\sum_{i \in \mathbf{F}_j} s_i$  approaches the normal distribution according to the central limit theorem, i.e.,  $\sum_{i \in \mathbf{F}_j} s_i \sim \mathcal{N}(N_j\mu_s, N_j\sigma_s^2)$ . As the sum of two independent Gaussians is also Gaussian,  $Y|H_1$  follows the normal distribution, i.e.,  $Y|H_1 \sim \mathcal{N}(N_j\mu_s + N_j\mu, N_j\sigma_s^2 + N_j\sigma^2)$ . Hence, the detection probability in the  $j^{\text{th}}$  unit detection is given by  $P_{Dj} = \mathbb{P}(Y \geq \eta|H_1) \simeq Q\left(\frac{\eta - N_j\mu_s - N_j\mu}{\sqrt{N_j \cdot \sigma_s^2 + \sigma^2}}\right)$ . By replacing  $\eta$  with the optimal detection threshold  $\eta^*$ , we have

$$P_{Dj} \simeq Q\left(\frac{\sigma}{\sqrt{\sigma_s^2 + \sigma^2}} \cdot Q^{-1}(\alpha) - \frac{\mu_s}{\sqrt{\sigma_s^2 + \sigma^2}} \cdot \sqrt{N_j}\right). \quad (4)$$

## 5.2 $\alpha$ -Delay of Fusion-based Detection

As discussed in Section 3.3, the process of detecting a target consists of a series of unit detections. Based on the performance modeling of each unit detection in Section 5.1, we now derive the  $\alpha$ -delay under the data fusion model.

In this section, we assume that there is no overlap between any two fusion ranges (as shown in Fig. 6). As a result, the sensor sets  $\{\mathbf{F}_j|j \geq 1\}$  are independent from each other. Such independence can significantly simplify the analysis. We now discuss the condition for no overlap between any two fusion ranges. Suppose the target moves at a constant speed of  $v$ , the no-overlap condition can be satisfied if  $vT > 2R$ . For instance, if the fusion range  $R$  is set to be 10 m and the target speed  $v$  is 5 m/s (i.e., 18 km/h) [11], the fusion ranges will not overlap as long as the detection period  $T$  is greater than 4 s. In Section 7.1, we extend the analysis to the case where fusion ranges may overlap.

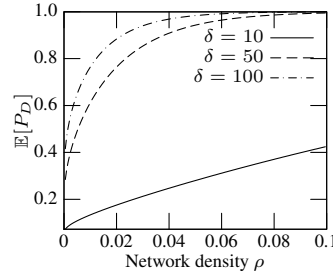


Fig. 7. Mean detection probability versus network density ( $R = 25$  m).

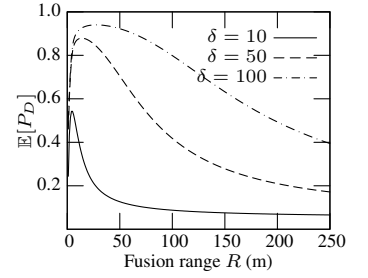


Fig. 8. Mean detection probability versus fusion range ( $\rho = 0.03$ ).

From (4),  $P_{Dj}$  is a function of  $N_j$ . When the sensor sets  $\{\mathbf{F}_j|j \geq 1\}$  are independent,  $\{P_{Dj}|j \geq 1\}$  are *i.i.d.* as the numbers of sensors involved in each unit detection (i.e.,  $\{N_j|j \geq 1\}$ ) are *i.i.d.* due to the Poisson process. We denote  $\mathbb{E}[P_D]$  as the mean of  $P_{Dj}$  for any  $j$ , i.e.,  $\mathbb{E}[P_D] = \mathbb{E}[P_{Dj}]$ ,  $\forall j$ . Intuitively, the intrusion detection can be viewed as a series of infinite Bernoulli trials and the success probability of each Bernoulli trial is  $\mathbb{E}[P_D]$ . Accordingly, the number of unit detections before (and including) the first successful unit detection follows the geometric distribution with a mean of  $1/\mathbb{E}[P_D]$ . Hence the  $\alpha$ -delay is given by the following theorem. The formal proof is in Appendix C, which can be found in the supplemental materials of this paper.

**Theorem 1.** Let  $\tau$  denote the  $\alpha$ -delay of fusion-based detection. If there is no overlap between any two fusion ranges,  $\tau = 1/\mathbb{E}[P_D]$ , where  $\mathbb{E}[P_D]$  is the average detection probability in any unit detection.

We now discuss how to compute  $\mathbb{E}[P_D]$  in Theorem 1. As  $P_{Dj}$  is a function of  $N_j$  and  $N_j$  follows the Poisson distribution, i.e.,  $N_j \sim \text{Poi}(\rho\pi R^2)$ ,  $\mathbb{E}[P_D]$  is given by

$$\mathbb{E}[P_D] = \sum_{N_j=0}^{\infty} P_{Dj} \cdot f_{\text{Poi}}(N_j|\rho\pi R^2), \quad (5)$$

where  $f_{\text{Poi}}(k|\lambda)$  is the probability density function (PDF) of the Poisson distribution  $\text{Poi}(\lambda)$ . Specifically,  $f_{\text{Poi}}(k|\lambda) = \lambda^k e^{-\lambda}/k!$ . Note that  $P_{Dj}$  in (5) is computed using (4).

Fig. 7 and Fig. 8 plot  $\mathbb{E}[P_D]$  versus network density  $\rho$  and fusion range  $R$ , respectively. From Fig. 7, we can see that  $\mathbb{E}[P_D]$  increases with  $\rho$ . Moreover, for a certain  $\rho$ ,  $\mathbb{E}[P_D]$  increases with the SNR. From Fig. 8, we can see that  $\mathbb{E}[P_D]$  is a concave function of fusion range  $R$  and there exists an optimal  $R$  that maximizes  $\mathbb{E}[P_D]$ . Intuitively, as the fusion range initially increases, more sensors contribute to the data fusion resulting in better sensing quality. However, as the fusion range becomes very large, the aggregate noise starts to cancel out the benefit because the target signal decreases rapidly with the distance from the target. In other words, the measurements of sensors far away from the target contain low-quality information and hence fusing them

lowers detection performance. However, because of the complicated relationship between the  $\alpha$ -delay and fusion range  $R$ , it is difficult to obtain the analytical optimal fusion range. In practice, we can choose the optimal fusion range according to numerical results.

## 6 IMPACT OF DATA FUSION ON REAL-TIME DETECTION

Many mission-critical real-time applications require detection delay to be as small as possible [2], [27]. As an asymptotic case, the  $\alpha$ -delay approaches one, i.e., any intruder can be detected almost surely in the first detection period after its appearance, which is referred to as the *instant detection*. As a smaller detection delay always requires more sensors, the network density for achieving instant detection is an important cost metric for mission-critical real-time sensor networks.

In this section, we investigate the required network density for achieving instant detection under both the disc and fusion models. According to Lemma 1 and Theorem 1, the network density under both models approaches infinity<sup>4</sup> when the  $\alpha$ -delay reduces to one. However, the speed that the network density increases is different. In this section, we study the ratio of network densities for instant detection under the two models, which characterize the relative cost of the two models when detection delay is minimized. The result provides important insights into understanding the limitation of the disc model and the impact of data fusion on the performance of real-time WSNs for intrusion detection.

### 6.1 Network Density for Achieving Instant Detection

In this section, we assume that the target discs and fusion ranges under the disc and fusion models do not overlap, respectively. In Section 7.1, we will generalize the analysis to the case where target discs or fusion ranges may overlap. We have the following lemma. The proof is in Appendix D, which can be found in the supplemental materials of this paper.

**Lemma 2.** *Let  $\rho_f$  and  $\rho_d$  denote the network densities for achieving  $\alpha$ -delay of  $\tau$  under the value fusion and disc models, respectively. If there is no overlap between target discs and fusion ranges under the two models, respectively, there exists  $\xi \in (0, 1)$  such that*

$$\frac{2}{\gamma^2 R^2} \cdot r^2 \leq \lim_{\tau \rightarrow 1^+} \frac{\rho_f}{\rho_d} \leq \frac{2}{\xi \gamma^2 R^2} \cdot r^2, \quad (6)$$

where  $\gamma = -\frac{\mu_s}{\sqrt{\sigma_s^2 + \sigma^2}}$ .

Note that according to the proof of Lemma 2,  $\xi$  is a function of  $\gamma$ . According to Lemma 2,  $\lim_{\tau \rightarrow 1^+} \rho_f/\rho_d$  is largely affected by the sensing range of a single sensor.

4. Numerically, the network density  $\rho$  will not be very large when the  $\alpha$ -delay approaches one. For instance, according to Lemma 1, suppose the sensing range  $r$  is 5 m, the  $\alpha$ -delay under the disc model is  $1 + 10^{-5}$  when  $\rho = 0.15$ .

According to (3), the sensing range  $r$  is determined by the requirements on false alarm rate and detection probability (i.e.,  $\alpha$  and  $\beta$ ), as well as the SNR  $\delta$ . As discussed in Section 4.2,  $\beta$  is a constant close to one. Accordingly, we only analyze the impacts of  $\alpha$  and  $\delta$  on the network density for achieving instant detection. We have the following theorem.

**Theorem 2.** *If there is no overlap between target discs and fusion ranges under the disc and value fusion models, respectively, for given path loss exponent  $k$ , the ratio of network densities for instant detection under the two models has an asymptotic tight bound of*

$$\lim_{\tau \rightarrow 1^+} \frac{\rho_f}{\rho_d} = \Theta \left( \left( \frac{\delta}{Q^{-1}(\alpha)} \right)^{2/k} \right). \quad (7)$$

*Proof:* In Lemma 2,  $\gamma$  depends on the SNR  $\delta$ , i.e.,

$$\gamma = -\frac{\mu_s}{\sqrt{\sigma_s^2 + \sigma^2}} = -\frac{S\mu_0}{\sqrt{S^2\sigma_0^2 + \sigma^2}} = -\frac{\mu_0}{\sqrt{\sigma_0^2 + \frac{1}{S^2}}},$$

where  $\mu_0$  and  $\sigma_0^2$  are constants given in Section 5.1. Moreover,  $\xi$  is a function of  $\gamma$ . Accordingly,  $\gamma$  and  $\xi$  are both constants when  $\delta$  is fixed or approaches infinity. Hence, according to Lemma 2, the tight bound of the density ratio is  $\lim_{\tau \rightarrow 1^+} \rho_f/\rho_d = \Theta(r^2)$ . As  $w^{-1}(x) = \Theta(x^{-1/k})$ , according to (3),  $r^2 = \Theta \left( \left( \frac{\delta}{Q^{-1}(\alpha)} \right)^{2/k} \right)$  for fixed  $\beta$ .

Therefore, we have (7).  $\square$

Theorem 2 suggests that, for a certain path loss exponent  $k$ , the relative cost for instant detection between the fusion and disc models depends on the required false alarm rate  $\alpha$  and SNR  $\delta$ . First, when  $\alpha \rightarrow 0$ ,  $Q^{-1}(\alpha) \rightarrow \infty$  and hence  $\lim_{\tau \rightarrow 1^+} \rho_f/\rho_d \rightarrow 0$ . It suggests that data fusion can significantly reduce network density when a small false alarm rate is required. Second,  $\lim_{\tau \rightarrow 1^+} \rho_f/\rho_d$  increases with  $\delta$ , which suggests that the advantage of data fusion diminishes as the SNR increases. Moreover, the path loss exponent  $k$  determines the order of density ratio with regard to the SNR. Intuitively, sensor collaboration is more advantageous when the SNR is low. However, when the SNR is sufficiently high, the detection performance of a single sensor is satisfactory and the collaboration among multiple sensors may be unnecessary.

### 6.2 Application of Results

In this section, we use two realistic examples to illustrate the implications of Theorem 2. They also provide several important insights into understanding the applicability of the disc model and the data fusion model in various application scenarios.

#### 6.2.1 Data fusion reduces network density

As  $\lim_{\tau \rightarrow 1^+} \rho_f/\rho_d \rightarrow 0$  when  $\alpha \rightarrow 0$ , if a small  $\alpha$  is required,  $\rho_f < \rho_d$  for instant detection, i.e., the fusion model requires lower network density than the disc model. In other words, data fusion is effective in

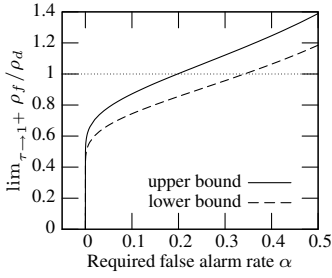


Fig. 9. Density ratio versus required false alarm rate ( $k = 2$ ,  $\delta = 50$ ,  $R = 37$  m).

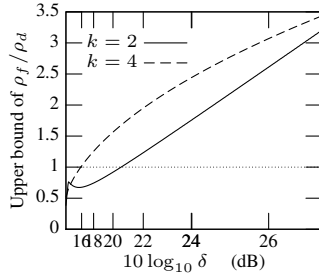


Fig. 10. Upper bound of density ratio versus SNR ( $\alpha = 0.1\%$ ).

reducing detection delay and false alarms. Fig. 9 plots the lower and upper bounds of the density ratio given by Lemma 2. We set the SNR  $\delta$  to be 50 (i.e., 17 dB) according to the measurements in the vehicle detection experiments based on MICA2 [28] and ExScal [25] motes. The fusion range  $R$  is optimized to be 37 m. From the figure, we can see that if  $\alpha < 0.2$ , the fusion model will outperform the disc model. In practice, most mission-critical surveillance systems require a small  $\alpha$ . For example, in the vehicle detection system [2] and the acoustic shooter localization system [27], the false alarm rates are tuned to be near zero. Therefore, data fusion can significantly reduce the network density for these mission-critical surveillance systems.

### 6.2.2 Disc model suffices for high-SNR detection

As  $\lim_{\tau \rightarrow 1^+} \rho_f / \rho_d$  increases with  $\delta$  for fixed  $\alpha$ , if the SNR is high enough such that  $\lim_{\tau \rightarrow 1^+} \rho_f / \rho_d > 1$ , the disc model is superior to the value fusion model in achieving instant detection. It implies that the disc model suffices when the SNR is sufficiently high. Fig. 10 plots the upper bound of density ratio versus SNR under various path loss exponents. From the figure, we can see linear and concave relationships between the density ratio and SNR when  $k$  is 2.0 and 4.0, respectively, which are consistent with Theorem 1. Moreover, if the SNR is sufficiently high (e.g., 22 dB), the disc model outperforms the value fusion model. However, the noise experienced by a sensor comes from various sources, e.g., the random disturbances in the environment and the electronic noise in the sensor's circuit. Thus, the SNR depends on the characteristics of targets, the environment, and the sensor device. In the vehicle detection experiments based on low-power motes, e.g., MICA2 [28] and ExScal [25], the SNRs are usually low to moderate ( $\leq 17$  dB). In such a case, value fusion can effectively reduce the network density required to achieve short detection delay and low false alarm rate.

## 7 EXTENSIONS

In this section, we generalize the results to address arbitrary target speed and short detection period. We then extend our analyses to address decision fusion model.

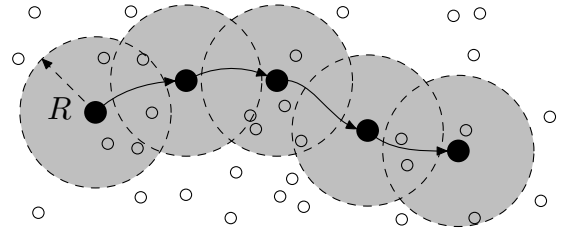


Fig. 11. The overlap case under the data fusion model. The void circles represent sensors; the solid circles represent the target in different sampling intervals; the dashed discs represent the fusion ranges.

### 7.1 Extension to General Target Speed and Detection Period

In previous sections, we assume that there is no overlap between any two target discs and fusion ranges under the disc and fusion models, respectively. However, fusion ranges may overlap if the target speed is low or the detection period  $T$  is short, as illustrated in Fig. 11. In this section, we will generalize the previous analyses without the no-overlap limitation. Recall the discussions in Sections 4.2 and 5.2, when there is no overlap, the unit detections are independent from each other. As a result, the index of first successful unit detection (i.e.,  $J$ ) follows the geometric distribution and the  $\alpha$ -delay can be computed as the mean of the geometric distribution. In contrast, when target discs or fusion ranges can overlap, the detection results in different unit detections are statistically *correlated* due to the possible common sensors shared by different unit detections. Hence,  $J$  does not follow the geometric distribution anymore. Therefore, the correlation among unit detections substantially complicates the analysis of  $\alpha$ -delay. As a result, it is difficult to obtain the closed-form formula of  $\alpha$ -delay. Instead, we aim to find the bound of  $\alpha$ -delay in this section. The lower bound of  $\alpha$ -delay under the disc model is given by the following lemma. The proof is in Appendix E, which can be found in the supplemental materials of this paper.

**Lemma 3.** Let  $\tau$  denote the  $\alpha$ -delay under the probabilistic disc model. We have  $\tau \geq \frac{1}{1 - e^{-\rho\pi r^2}}$ , where  $r$  is given by (3).

Compared with the results in Lemmas 1 and 3, we can see that the  $\alpha$ -delay is minimized for the no-overlap case. Intuitively, the area covered by the union of target discs is maximized in the no-overlap case, which yields the maximum overall detection probability for a given number of detection periods and in turn leads to the minimum detection delay.

The upper bound of  $\alpha$ -delay under the data fusion model is given by the following theorem. The proof is in Appendix F, which can be found in the supplemental materials of this paper.

**Theorem 3.** Let  $\tau$  denote the  $\alpha$ -delay of fusion-based detection. We have  $\tau \leq \mathbb{E}[1/P_D]$ , where  $P_D$  is the detection probability in any unit detection.

As  $1/P_D$  is a convex function of  $P_D$ , according to Jensen's inequality,  $\mathbb{E}[1/P_D] \geq 1/\mathbb{E}[P_D]$ , where  $1/\mathbb{E}[P_D]$  is the  $\alpha$ -delay when there is no overlap between any two fusion ranges. We now discuss how to compute  $\mathbb{E}[1/P_D]$  in Theorem 3. As  $P_{Dj}$  is a function of  $N_j$  which follows the Poisson distribution, i.e.,  $N_j \sim \text{Poi}(\rho\pi R^2)$ ,  $\mathbb{E}[1/P_D]$  can be numerically computed by averaging  $\frac{1}{P_{Dj}}$  over the distribution of  $N_j$ .

With the lower and upper bounds of  $\alpha$ -delay under the disc and fusion models, respectively, we can derive the asymptotic bound of ratio of network densities required by the two models to achieve instant detection. As it is more challenging to handle the expression  $\mathbb{E}[1/P_D]$  in Theorem 3 than  $\mathbb{E}[P_D]$  in Theorem 1, compared with Section 6.1, we will employ substantially different technique to analyze the density ratio. We have the following theorem. The proof is in Appendix G, which can be found in the supplemental materials of this paper.

**Theorem 4.** *Let  $\rho_f$  and  $\rho_d$  denote the network densities for achieving  $\alpha$ -delay of  $\tau$  under the value fusion and disc models, respectively. For given path loss exponent  $k$ , the ratio of network densities for instant detection has an asymptotic upper bound of*

$$\lim_{\tau \rightarrow 1^+} \frac{\rho_f}{\rho_d} = \mathcal{O} \left( \left( \frac{\delta}{Q^{-1}(\alpha)} \right)^{2/k} \right). \quad (8)$$

Different from the result in Theorem 2 which is the asymptotic *tight* bound of the density ratio, Theorem 4 gives the asymptotic *upper* bound. In Section 8, we will compare the density ratios under the overlap and no-overlap cases through simulations. Moreover, as target speed is an important factor of the overlap/no-overlap condition, we also evaluate the impact of target speed on the density ratio.

## 7.2 Real-time Detection under Decision Fusion Model

In this section, we extend our analysis to a decision fusion model. In decision fusion scheme, each sensor makes a *local* decision based on its measurements and transmits its decision to the cluster head, which makes a *system* decision according to the local decisions. Due to its low communication overhead, decision fusion is often preferred in bandwidth-constrained sensor systems. We adopt a decision fusion model as follows. Each sensor  $i$  in  $\mathbf{F}(P)$  makes a local decision  $I_i$  by comparing its measurement  $y_i$  against a *local threshold*  $\lambda$ . If  $y_i \geq \lambda$ ,  $I_i = 1$ ; otherwise,  $I_i = 0$ . Let  $\Lambda$  denote the number of positive local decisions, i.e.,  $\Lambda = \sum_{i \in \mathbf{F}(P)} I_i$ . The cluster head makes a system detection decision by a threshold testing, i.e., given a *system threshold*  $\theta \in (0, 1)$ , if  $\frac{\Lambda}{N(P)} \geq \theta$ , the cluster head decides  $H_1$ ; otherwise, it decides  $H_0$ . By setting  $\theta = \frac{1}{2}$  or  $\theta = 1$ , the decision fusion model is the majority rule or AND rule, respectively. Such a decision fusion model has been widely employed in previous analytical studies [1], [15], [20], [22] and real systems [2].

We now analyze the performance of real-time detection under the decision fusion model. In the absence of target, the local false alarm rate of sensor  $i$ , denoted by  $P_F^i$ , is  $P_F^i = \mathbb{P}(y_i \geq \lambda|H_0) = Q\left(\frac{\lambda - \mu}{\sigma}\right)$ . Note that all sensors have the same local false alarm rate and thus we denote  $P_F^i = \alpha_0$ . In the  $j^{\text{th}}$  unit detection, the number of positive local decisions, i.e.,  $\Lambda|H_0$ , follows a Binomial distribution. Formally,  $\Lambda|H_0 \sim \text{Bin}(N_j, \alpha_0)$ , where  $N_j$  is the number of sensors within the fusion range in the  $j^{\text{th}}$  unit detection. However, the system false alarm rate under the binomial distribution is complicated [20]. We have proved in [20] that if  $N_j$  is large enough, the system false alarm rate in the  $j^{\text{th}}$  unit detection can be approximated by  $P_{Fj} = \mathbb{P}(\Lambda \geq \theta N_j|H_0) \simeq Q\left(\frac{\theta N_j - N_j \alpha_0}{\sqrt{N_j \alpha_0 - N_j \alpha_0^2}}\right)$ . In order to bound system false alarm rate, letting  $P_{Fj} = \alpha$  yields a quadratic equation with respect to  $\alpha_0$ , which has two distinct roots. We can compute the local threshold  $\lambda$  with the smaller root of  $\alpha_0$  within  $(0, 1)$ .

In the presence of target, the local detection probability of sensor  $i$ , denoted by  $P_D^i$ , is  $P_D^i = \mathbb{P}(y_i \geq \lambda|H_1) = Q\left(\frac{\lambda - \mu - s_i}{\sigma}\right)$ . As sensors receive different signal energies, their local decisions are independent but not identically distributed Bernoulli random variables. As proved in [20],  $\Lambda|H_1$  approximately follows the normal distribution according to Lyapunov's central limit theorem, where the system detection probability can be calculated by

$$P_{Dj} \simeq Q\left(\frac{\theta N_j - \sum_{i \in \mathbf{F}_j} P_D^i}{\sqrt{\sum_{i \in \mathbf{F}_j} P_D^i - \sum_{i \in \mathbf{F}_j} (P_D^i)^2}}\right). \quad (9)$$

In (9),  $\sum_{i \in \mathbf{F}_j} P_D^i$  is a random variable that follows a complicated compound distribution, which has no analytical CDF. We now analyze the bounds of  $P_{Dj}$ . Let  $P_D^{\min}$  and  $P_D^{\max}$  denote the lower and upper bounds of  $P_D^i$ , which are  $P_D^{\min} = Q\left(\frac{\lambda - \mu - S w(R)}{\sigma}\right)$  and  $P_D^{\max} = Q\left(\frac{\lambda - \mu - S}{\sigma}\right)$ , respectively. It has been shown in [20] that  $P_{Dj}$  given by (9) increases with  $\sum_{i \in \mathbf{F}_j} P_D^i$  with high probability. Therefore, the lower and upper bounds of  $P_{Dj}$  are given by  $Q\left(\frac{\theta - P_D^{\min}}{\sqrt{P_D^{\min} - (P_D^{\min})^2}} \cdot \sqrt{N_j}\right)$  and  $Q\left(\frac{\theta - P_D^{\max}}{\sqrt{P_D^{\max} - (P_D^{\max})^2}} \cdot \sqrt{N_j}\right)$ , respectively. Hence, there exists  $\gamma \in \left[\frac{\theta - P_D^{\max}}{\sqrt{P_D^{\max} - (P_D^{\max})^2}}, \frac{\theta - P_D^{\min}}{\sqrt{P_D^{\min} - (P_D^{\min})^2}}\right]$  such that  $P_{Dj} = Q(\gamma \sqrt{N_j})$ . Moreover, it is easy to verify that  $\gamma = \Theta\left(-\frac{1}{\sqrt{\Phi(-\delta)}}\right)$ , where  $\Phi(x) = 1 - Q(x)$ .

We now extend previous analytical results to the decision fusion model. Theorems 1 and 3 hold for any data fusion model if the unit detections are identically distributed. Hence, they hold for the decision fusion model in this section. Moreover, under both the value and decision fusion models, the relationship between  $P_{Dj}$  and  $N_j$  is identical in the asymptotic case (i.e.,  $P_{Dj} = Q(\gamma \sqrt{N_j})$ ). Therefore, Lemma 2 holds for the decision fusion model as well. However, different from

the value fusion model,  $\gamma$  for the decision fusion model is unbounded when  $\delta \rightarrow \infty$ . The following theorem extends Theorem 4 to the decision fusion model.

**Theorem 5.** *When decision fusion model is assumed, the relationship between  $\rho_f$  and  $\rho_d$  satisfies*

$$\lim_{\tau \rightarrow 1^+} \frac{\rho_f}{\rho_d} = \mathcal{O} \left( e^{-\delta} \cdot \left( \frac{\delta}{Q^{-1}(\alpha)} \right)^{2/k} \right). \quad (10)$$

*Proof:* Under the decision fusion model,  $\gamma = \Theta \left( -\frac{1}{\sqrt{\Phi(-\delta)}} \right)$ . Moreover,  $\Phi(x) \leq \sqrt{\frac{2}{\pi}} e^{\frac{x^2}{2}}$  for  $x \leq -1$ . Hence,  $\frac{1}{\gamma^2} = \Theta(\Phi(-\delta)) = \mathcal{O}(e^{-\delta})$ . According to the proof of Theorem 4,  $\lim_{\tau \rightarrow 1^+} \frac{\rho_f}{\rho_d} \leq \frac{2}{\gamma^2 \xi R^2} \cdot r^2$ , where  $\xi$  is any constant in  $(0, 1)$ . By replacing  $\frac{1}{\gamma^2} = \mathcal{O}(e^{-\delta})$  and  $r^2 = \Theta \left( \left( \frac{\delta}{Q^{-1}(\alpha)} \right)^{2/k} \right)$ , we have (10).  $\square$

From Theorem 5, the impact of  $\alpha$  on the density ratio is same for both the value and decision fusion models. Specifically, data fusion can significantly reduce network density when a small false alarm rate is required. However, different from Theorems 2 and 4, the density ratio decreases with  $\delta$ , which suggests that the decision fusion model is more effective than the value fusion model for achieving short detection delay in the case of high SNRs. The intuition behind this result is as follows. When the SNR is high, the local detection at a sensor can largely reduce the impact of noise. Moreover, the decision fusion of multiple sensors will further improve the system result. In contrast, under the value fusion model, the noises from sensors are still aggregated at the cluster head. Therefore, the value fusion model becomes less effective than the decision fusion model when the SNR is high. However, this paper is focused on arguing the advantages of collaborative data fusion with regard to the disc model in achieving real-time detection. The extensive comparison of data fusion models is left for our future work. The simulation results in Section 8 validates Theorem 5.

## 8 PERFORMANCE EVALUATION

In this section, we conduct extensive simulations based on real data traces as well as synthetic data to evaluate the real-time detection performance in non-asymptotic and asymptotic cases, respectively.

### 8.1 Trace-driven Simulations

We first conduct simulations using the data traces collected in a real vehicle detection experiment [11]. In the experiment, 75 WINS NG 2.0 nodes are deployed to detect military vehicles driving through the surveillance region. We refer to [11] for detailed setup of the experiment. The dataset used in our simulations includes the ground truth data and the acoustic time series recorded by 20 nodes when a vehicle drives through. The ground truth data include the positions of sensors and the trajectory of the vehicle.

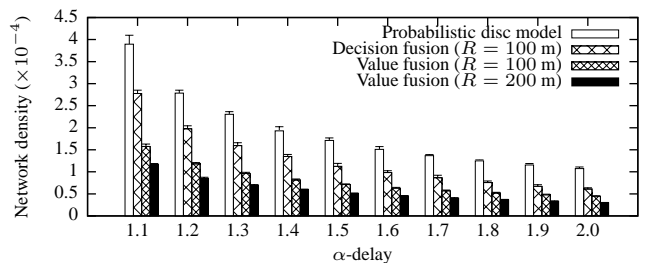


Fig. 12. The network density versus achieved  $\alpha$ -delay.

Sensors' sensing ranges under the probabilistic disc model are determined individually to meet the detection performance requirements ( $\alpha = 5\%$  and  $\beta = 95\%$ ). The resulted sensing ranges are from 22.5 m to 59.2 m with the average of 43.2 m. Such a significant variation is due to several issues including poor calibration and complex terrain. The sensors are deployed uniformly into a large field and periodically detect the target. The target initially appears at the origin, and moves along the  $X$ -axis at a speed of 10 m/s. The detection period  $T$  is set to be 60 s. Each sensor in the simulation is associated with a real sensor chosen at random. When a sensor makes a measurement, its reading is set to be the energy gathered by the associated real sensor at a similar distance to vehicle in the data trace. Under the disc model, once the target enters the sensing range of a sensor, the sensor makes a detection decision by comparing its measurement against the detection threshold  $t$  derived in Section 4.1. Under the fusion model, sensors fuse their measurements or local decisions to detect the target as discussed in Section 3.2. For the decision fusion model, we adopt the majority rule, i.e.,  $\theta = \frac{1}{2}$ . We conduct 500 runs with different random sensor deployments. The  $\alpha$ -delay is computed as the average number of detection periods before the target is first detected in each run.

Fig. 12 plots the network density versus the achieved  $\alpha$ -delay under various settings. We can see that the data fusion models are more effective than the disc model for achieving short  $\alpha$ -delay. In particular, the value fusion model with a fusion range of 100 m saves more than 50% sensors when the  $\alpha$ -delay is less than 2. We note that the average number of sensors taking part in data fusion is within 20 and hence will not introduce high communication overhead. Moreover, as value fusion often has better detection performance than decision fusion [1], we can see from Fig. 12 that the decision fusion model requires more sensors than the value fusion model.

### 8.2 Simulations based on Synthetic Data

#### 8.2.1 Simulation Settings and Methodology

Both the mean and variance of the noise generator (i.e.,  $\mu$  and  $\sigma^2$ ) are set to be 1. Except those explicitly specified, the default settings of SNR and fusion range are 50 (i.e., 17 dB) and 25 m, respectively. Note that the setting of SNR is according to the measurements in the vehicle detection experiments based on motes [25], [28].

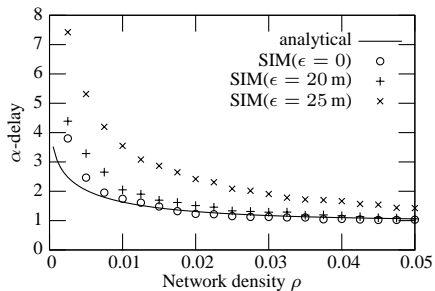


Fig. 13.  $\alpha$ -delay versus network density under value fusion model.

The sensors are deployed uniformly into a large field and periodically detect the target. The target initially appears at the origin, and moves along the  $X$ -axis at a speed of  $2R$  per detection period. Under the fusion model, we consider the target localization error as follows. Suppose the real target position is at  $P(x, y)$  when sensors take measurements, while the target position localized by the network is at  $P'(x + \epsilon \cos \theta, y + \epsilon \sin \theta)$ , where  $\epsilon$  is a specified constant and  $\theta$  is picked uniformly from  $[0, 2\pi)$ . Sensors within the fusion range centered at  $P'$  fuse their measurements and make the detection decision. Under the disc model, the sensing range  $r$  is computed according to (3). Once the target enters the sensing range of a sensor, the sensor makes a detection decision by comparing its measurement against the detection threshold  $t$  derived in Section 4.1. We conduct 500 runs with different random sensor deployments. The  $\alpha$ -delay is computed as the average number of detection periods before the target is first detected in each run. We also evaluate the impact of the overlap/no-overlap condition by comparing the simulation results under the overlap and no-overlap cases. For the overlap case, the target moves  $\frac{R}{2}$  and  $\frac{r}{2}$  in each detection period under the fusion and disc models, respectively; for the no-overlap case, it moves  $2R$  and  $2r$ , respectively.

### 8.2.2 Simulation Results

We first evaluate the analytical  $\alpha$ -delay of fusion-based detection under the no-overlap case, which is given by Theorem 1. Meanwhile, we also evaluate the impact of localization error on the result. Fig. 13 plots the  $\alpha$ -delay versus the network density under the value fusion model. The curve labeled with “analytical” plots the  $\alpha$ -delay computed according to Theorem 1 and Eq. (5). The data points labeled with “SIM( $\epsilon$ )” represent the simulation results with a constant localization error  $\epsilon$ . From the figure, we can see that the  $\alpha$ -delay decreases with the network density. The simulation result without localization error (i.e.,  $\epsilon = 0$ ) confirms the analytical result when the network density is greater than 0.01. When  $\rho$  is smaller than 0.01, the simulation result starts to deviate from the analytical result. This is due to the approximation made in the derivation of  $P_D$  in Section 5.1. However, we can see that the maximum error between the analytical and simulation results falls within

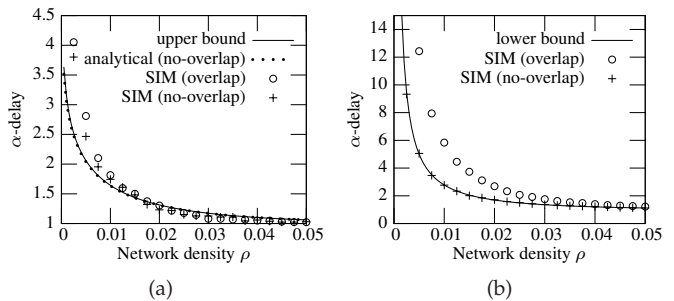


Fig. 14.  $\alpha$ -delay versus network density. (a) Value fusion model. (b) Disc model.

one detection period. Fig. 13 also shows that the impact of localization error is small. The simulation result has a considerable deviation from the analytical result only when the localization error is equal to the fusion range (25 m). In such a case, the target falls completely outside of the fusion range. Moreover, the impact of localization error diminishes as the network density increases. This result demonstrates the robustness of our analysis with respect to localization error, especially in achieving instant detection.

The second set of simulations evaluate the impact of overlap/no-overlap condition on the  $\alpha$ -delay under the disc and fusion models, respectively. Fig. 14(a) plots the  $\alpha$ -delay versus the network density under the value fusion model. The curves labeled with “analytical (no-overlap)” and “upper bound” plot the  $\alpha$ -delay under the no-overlap case (given by Theorem 1) and its upper bound (given by Theorem 3), respectively. We can see that the two analytical results are very close. The other two curves plot the simulation results for the overlap and no-overlap cases, respectively. The simulation results closely match the analytical results when the network density is greater than 0.02. When  $\rho$  is smaller than 0.01, the deviation between the analytical and simulation results is due to the approximation made in the derivation of  $P_D$ . Moreover, we can see from Fig. 14(a) that the overlap/no-overlap condition has little impact on the  $\alpha$ -delay under the fusion model. Fig. 14(b) plots the  $\alpha$ -delay under the disc model. Note that the lower bound given by Lemma 3 is also the analytical result of  $\alpha$ -delay under the no-overlap case given by Lemma 1. We can see that the simulation results confirm the analytical results under the disc model. Moreover, the  $\alpha$ -delay significantly increases under the overlap case. Hence, the overlap/no-overlap condition has significant impact on the  $\alpha$ -delay under the disc model.

We now evaluate the impact of false alarm rate on the density ratio. Fig. 15(a) plots the ratio of network densities required by the value fusion and disc models to achieve the same  $\alpha$ -delay given various false alarm rates. Fig. 15(b) plots the corresponding results for the decision fusion model. We can see from Fig. 15(a) that the disc model requires more than twice sensors when the  $\alpha$ -delay approaches to one. Both for the value and decision

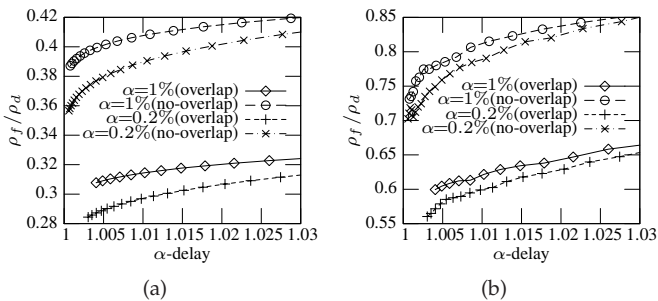


Fig. 15. Density ratio versus  $\alpha$ -delay given different  $\alpha$  (SNR = 10 dB). (a) Value fusion. (b) Decision fusion.

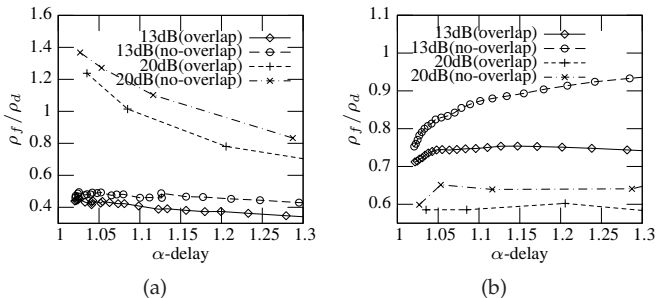


Fig. 16. Density ratio versus  $\alpha$ -delay given different SNR ( $\alpha = 1\%$ ). (a) Value fusion. (b) Decision fusion.

fusion models, the density ratio decreases if a lower  $\alpha$  is required, which is consistent with Theorems 2, 4 and 5. Moreover, from the two figures, we can see that the density ratio under the overlap case is smaller than that under the no-overlap case. This is consistent with our observation in the previous set of simulations, i.e., the overlap condition has little impact on the fusion model while leads to significant increase of  $\alpha$ -delay under the disc model.

We then evaluate the impact of SNR on the density ratio. Fig. 16(a) plots the ratio of network densities required by the value fusion and disc models given various SNRs. Fig. 16(b) plots the corresponding results for the decision fusion model. From Fig. 16(a), we can see that the density ratio increases with SNR, which is consistent Theorems 2 and 4. For instance, if the SNR is 13 dB, the density ratio  $\rho_f/\rho_d$  is about 0.5 when the  $\alpha$ -delay reduces to one. However, if the SNR increases to 20 dB,  $\rho_f/\rho_d$  is greater than 1.2 and hence the disc model requires fewer sensors than the fusion model. In contrast, as shown in Fig. 16(b), the decision fusion model can reduce the density ratio when SNR increases, which is consistent with Theorem 5. Moreover, from Fig. 16, we can see that value and decision fusion models are suitable for low and high SNR scenarios, respectively.

As target speed is an important factor of the overlap/no-overlap condition, we finally evaluate its impact on the density ratio. Fig. 17 shows the density ratio versus the target speed. We can see that the density ratio significantly increases when the target speed increases from  $\frac{r}{20}$  to  $2r$ . This is due to the significant impact of

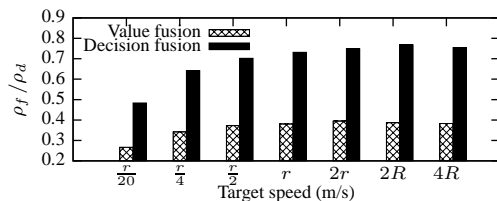


Fig. 17. Density ratio versus target speed (SNR = 13 dB,  $\alpha = 5\%$ ,  $\tau = 1.05$ ,  $r = 2.25$  m,  $R = 8$  m,  $T = 1$  s).

overlap condition on the disc model, as observed in Fig. 14(b). Hence, the data fusion models are more robust than the disc model in detecting slowly moving targets.

## 9 CONCLUSION

In this paper, we study the impact of data fusion on real-time detection in WSNs through the performance comparison between the disc model and various data fusion models. Our results show that data fusion is effective in achieving stringent performance requirements such as short detection delay and low false alarm rate. Moreover, value and decision fusion models are suitable for low and high SNR scenarios, respectively. Our results help understand the applicability of the disc and data fusion models, and hence provide important guidelines for the design of real-time WSNs for intrusion detection. This paper assumes the Poisson process model for sensor deployment. In our future work, we will extend the study to address other deployment models such as the grid deployment.

## ACKNOWLEDGMENT

This work is supported, in part, by the National Science Foundation under CAREER grants CNS-0954039 and CNS-0953620.

## REFERENCES

- [1] P. Varshney, *Distributed Detection and Data Fusion*. Springer, 1996.
- [2] T. He, S. Krishnamurthy, J. A. Stankovic, T. Abdelzaher, L. Luo, R. Stoleru, T. Yan, L. Gu, J. Hui, and B. Krogh, "Energy-efficient surveillance system using wireless sensor networks," in *The 2nd International Conference on Mobile Systems, Applications, and Services (MobiSys)*, 2004.
- [3] T. He, P. A. Vicaire, T. Yan, L. Luo, L. Gu, G. Zhou, R. Stoleru, Q. Cao, J. A. Stankovic, and T. Abdelzaher, "Achieving real-time target tracking using wireless sensor networks," in *12th IEEE Real-Time and Embedded Technology and Applications Symposium (RTAS)*, 2006.
- [4] S. Bapat, V. Kulathumani, and A. Arora, "Analyzing the yield of ExScal, a large-scale wireless sensor network experiment," in *13th IEEE International Conference on Network Protocols (ICNP)*, 2005.
- [5] Q. Cao, T. Yan, J. Stankovic, and T. Abdelzaher, "Analysis of target detection performance for wireless sensor networks," in *International Conference on Distributed Computing in Sensor Systems (DCOSS)*, 2005.
- [6] O. Dousse, C. Tavouraris, and P. Thiran, "Delay of intrusion detection in wireless sensor networks," in *The 7th ACM International Symposium on Mobile Ad Hoc Networking and Computing (MobiHoc)*, 2006.
- [7] L. Lazos, R. Poovendran, and J. A. Ritcey, "Probabilistic detection of mobile targets in heterogeneous sensor networks," in *International Conference on Information Processing in Sensor Networks (IPSN)*, 2007.

- [8] N. Bisnik, A. Abouzeid, and V. Isler, "Stochastic event capture using mobile sensors subject to a quality metric," in *The 12th Annual International Conference on Mobile Computing and Networking (MobiCom)*, 2006.
- [9] B. Liu and D. Towsley, "A study of the coverage of large-scale sensor networks," in *The 1st IEEE International Conference on Mobile Ad-Hoc and Sensor Systems (MASS)*, 2004.
- [10] P. Brass, "Bounds on coverage and target detection capabilities for models of networks of mobile sensors," *ACM Transactions on Sensor Networks*, vol. 3, no. 2, 2007.
- [11] M. F. Duarte and Y.-H. Hu, "Vehicle classification in distributed sensor networks," *Journal of Parallel and Distributed Computing*, vol. 64, no. 7, 2004.
- [12] R. Tan, G. Xing, J. Chen, W.-Z. Song, and R. Huang, "Quality-driven volcanic earthquake detection using wireless sensor networks," in *The 31st IEEE Real-Time Systems Symposium (RTSS)*, 2010.
- [13] D. Li, K. Wong, Y.-H. Hu, and A. Sayeed, "Detection, classification and tracking of targets in distributed sensor networks," *IEEE Signal Processing Magazine*, vol. 19, no. 2, 2002.
- [14] M. Duarte and Y.-H. Hu, "Distance based decision fusion in a distributed wireless sensor network," in *The 2nd International Workshop on Information Processing in Sensor Networks (IPSN)*, 2003.
- [15] T. Clouqueur, K. K. Saluja, and P. Ramanathan, "Fault tolerance in collaborative sensor networks for target detection," *IEEE Transactions on Computers*, vol. 53, no. 3, 2004.
- [16] X. Sheng and Y.-H. Hu, "Maximum likelihood multiple-source localization using acoustic energy measurements with wireless sensor networks," *IEEE Transactions on Signal Processing*, vol. 53, no. 1, 2005.
- [17] D. Li and Y.-H. Hu, "Energy based collaborative source localization using acoustic micro-sensor array," *EUROSIP Journal on Applied Signal Processing*, no. 4, 2003.
- [18] J. Kotecha, V. Ramachandran, and A. Sayeed, "Distributed Multitarget Classification in Wireless Sensor Networks," *IEEE Journal on Selected Areas in Communications (J-SAC)*, vol. 23, no. 4, 2005.
- [19] Z. Yuan, R. Tan, G. Xing, C. Lu, Y. Chen, and J. Wang, "Fast sensor placement algorithms for fusion-based target detection," in *The 29th IEEE Real-Time Systems Symposium (RTSS)*, 2008.
- [20] R. Tan, G. Xing, J. Wang, and H. C. So, "Exploiting reactive mobility for collaborative target detection in wireless sensor networks," *IEEE Transactions on Mobile Computing*, vol. 9, no. 3, 2010.
- [21] G. Xing, J. Wang, K. Shen, Q. Huang, X. Jia, and H. C. So, "Mobility-assisted spatiotemporal detection in wireless sensor networks," in *The 28th IEEE International Conference on Distributed Computing Systems (ICDCS)*, 2008.
- [22] R. Niu and P. K. Varshney, "Distributed detection and fusion in a large wireless sensor network of random size," *EURASIP Journal on Wireless Communication and Networking*, vol. 4, 2005.
- [23] G. Xing, R. Tan, B. Liu, J. Wang, X. Jia, and C.-W. Yi, "Data fusion improves the coverage of wireless sensor networks," in *The 15th Annual International Conference on Mobile Computing and Networking (MobiCom)*, 2009.
- [24] M. Hata, "Empirical formula for propagation loss in land mobile radio services," *IEEE Transactions on Vehicular Technology*, vol. 29, 1980.
- [25] L. Gu, D. Jia, P. Vicaire, T. Yan, L. Luo, A. Tirumala, Q. Cao, T. He, J. Stankovic, T. Abdelzaher, and H. Bruce, "Lightweight detection and classification for wireless sensor networks in realistic environments," in *The 3rd ACM Conference on Embedded Networked Sensor Systems (SenSys)*, 2005.
- [26] W.-P. Chen, J. C. Hou, and L. Sha, "Dynamic clustering for acoustic target tracking in wireless sensor networks," *IEEE Transactions on Mobile Computing*, vol. 3, no. 3, 2004.
- [27] P. Volgyesi, G. Balogh, A. Nadas, C. Nash, and A. Ledeczi, "Shooter Localization and Weapon Classification with Soldier-Wearable Networked Sensors," in *The 5th International Conference on Mobile Systems, Applications, and Services (MobiSys)*, 2007.
- [28] B. P. Flanagan and K. W. Parker, "Robust distributed detection using low power acoustic sensors," The MITRE Corporation, Tech. Rep., 2005.



**Rui Tan** received the B.S. and M.S. degrees in automation from Shanghai Jiao Tong University, China, in 2004 and 2007, respectively. He received the Ph.D. degree in computer science from City University of Hong Kong in 2010. He is currently a postdoctoral researcher at Michigan State University. His research interests include collaborative sensing in wireless sensor networks and cyber-physical systems. He is a student member of the IEEE.



**Guoliang Xing** received the B.S. degree in electrical engineering and the M.S. degree in computer science from Xi'an Jiao Tong University, China, in 1998 and 2001, respectively, and the M.S. and D.Sc. degrees in computer science and engineering from Washington University in St. Louis, in 2003 and 2006, respectively. He is an assistant professor in the Department of Computer Science and Engineering at Michigan State University. From 2006 to 2008, he was an assistant professor of computer science at

City University of Hong Kong. He served on a number of technical program committees and held several workshop organization positions including the program co-chairs of the First ACM International Workshop on Heterogeneous Sensor and Actor Networks (HeterSanet) 2008 and the Workshop on Wireless Ad hoc and Sensor Networks (WWASN) 2008 and 2009. He is an NSF CAREER Award recipient in 2010. He received the Best Paper Award at the 18th IEEE International Conference on Network Protocols (ICNP) in 2010. His research interests include wireless sensor networks, mobile systems, and cyber-physical systems.



**Jianping Wang** received the B.S. and M.S. degrees in computer science from Nankai University, China, in 1996 and 1999, respectively, and the Ph.D. degree from the University of Texas at Dallas in 2003. She is currently an assistant professor of computer science at City University of Hong Kong. Prior to joining City University of Hong Kong, she worked at the University of Mississippi and Georgia Southern University. Her research interests are optical networks, multi-cast, dependable networking, wireless networks,

and the integration of optical networks and wireless networks. She is a member of the IEEE.



**Benyuan Liu** received the Ph.D. degree in computer science from the University of Massachusetts, Amherst. He is currently an associate professor of computer science at University of Massachusetts Lowell. His research interests are in the area of protocol design and performance modeling of wireless ad hoc and sensor networks. He served as technical program co-chair of WASA 2009 and Cross-layer Design and Optimization Track of IEEE ICCCN 2008, and served on technical program committee for

numerous computer networking conferences.